HHS Public Access

Author manuscript

Cell Rep Phys Sci. Author manuscript; available in PMC 2025 March 13.

Published in final edited form as:

Cell Rep Phys Sci. 2024 December 18; 5(12): . doi:10.1016/j.xcrp.2024.102336.

De novo design of a mechano-pharmaceutical screening platform against formation of individual beta-amyloid oligomers

Shankar Pandey[1,9], **Mathias Bogetoft Danielsen**[2,9], **Yuan Xiang**[3,4], **Zhilei Zhang**[1], **Grinsun Sharma**[7], **Byeong Tak Jeon**[5], **Shixi Song**[2], **Yitong Hao**[2], **Gunan Zhang**[3], **Niels Johan Christensen**[6], **Kasper Kildegaard Sørensen**[6], **Pernille Harris**[6], **Pravin Pokhrel**[1], **Richard Cunningham**[8], **Min-Ho Kim**[5], **Yongsheng Leng**[3], **Chenguang Lou**[2,*], **Hanbin Mao**[1,10,*]

[1]Department of Chemistry and Biochemistry, Kent State University, Kent, OH 44242, USA

[2]Department of Physics, Chemistry, and Pharmacy, University of Southern Denmark, Campusvej 55, 5230 Odense M, Denmark

[3]Department of Mechanical and Aerospace Engineering, The George Washington University, Washington, DC 20052, USA

[4]Department of Mathematical & Physical Sciences, Chengdu University of Technology, Chengdu 610059, China

[5]Department of Biological Sciences, Kent State University, Kent, OH 44242, USA

[6]Department of Chemistry, University of Copenhagen, Universitetsparken 5, 2100 Copenhagen, Denmark

[7]School of Biomedical Sciences, Kent State University, Kent, OH 44242, USA

[8]ATDBio, Magdalen Centre, Oxford Science Park, 1 Robert Robinson Avenue, Oxford OX4 4GA, UK

[9]These authors contributed equally

[10]Lead contact

SUMMARY

*Correspondence: chenguang@sdu.dk (C.L.), hmao@kent.edu (H.M.).

AUTHOR CONTRIBUTIONS

H.M. and C.L. conceptualized the research. H.M. and S.P. designed the single-molecule experiments. S.P. and Z.Z. carried out the single-molecule experiments. M.B.D. synthesized the amino-modified ONs, ONs-alkyne, ONs-C-5, and POCs. Y.X., G.Z., and Y.L. performed the molecular simulations of FF-dimer unfolding. K.K.S. provided the azidohexanoyl-FF-NH_2. M.B.D. and S.S. carried out the synthesis and purification of H-FF-OH and the full-length $A\beta_{1\text{-}42}$ peptide. G.S. and B.T.J. performed the cell viability experiments. S.P. and Z.Z. conducted the turbidity assays. R.C. conducted the electrospray ionization-mass spectrometry characterization of ONs-C-5 and POCs. N.J.C. carried out the MD simulation and SAXS fitting. P.H. performed the SAXS measurement and raw data analysis. S.S. and Y.H. conducted the ThT assay experiments. S.P., M.B.D., C.L., and H.M. carried out the results analysis. C.L. and H.M. supervised the execution of the experiments. S.P., M.B.D., G.S., Y.L., C.L., and H.M. wrote the original manuscript draft. All authors contributed to finalizing the manuscript.

DECLARATION OF INTERESTS

The authors declare competing interests of the single-molecule screening technology and the tested small-molecule hit compounds, including inhibitors and promoters.

SUPPLEMENTAL INFORMATION

Supplemental information can be found online at https://doi.org/10.1016/j.xcrp.2024.102336.

Small molecules that can reduce the neurotoxic beta-amyloid (Aβ) aggregates in the brain provide a potential treatment for Alzheimer disease (AD). Most screening methods for small-molecule hits focus on the overall Aβ aggregations without a specific target, such as the very first association step (i.e., nucleation) *en route* to the Aβ oligomers. Located in the middle of a full-length Aβ peptide, $A\beta_{19–20}$ (diphenylalanine or FF) nucleates the neurotoxic Aβ oligomer formation. Here, we innovate a single-molecule screen method in optical tweezers by targeting the nucleation process in Aβ aggregation, namely FF-dimerization. With a 121-compound National Institutes of Health (NIH) library, we identify 12 inhibitors and 8 stimulants that can inhibit/promote $A\beta_{19–20}$ dimerization significantly. The representative hits are subjected to the thioflavin T and cell toxicity assays to confirm their inhibiting or stimulating activities. By replacing FF with longer Aβ sequences, our single-molecule platform may identify more specific and potent small molecules to fight AD.

Graphical abstract

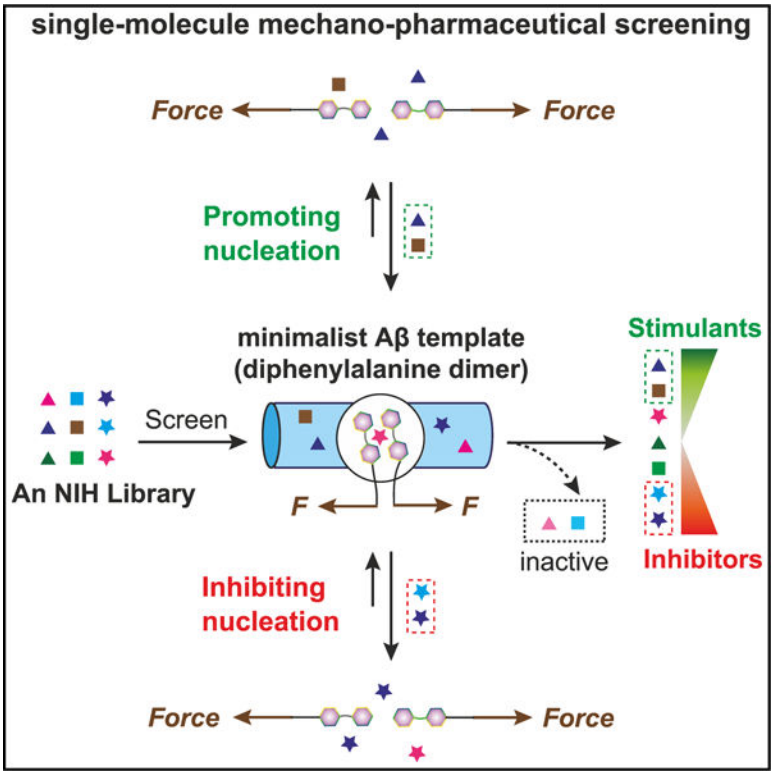

In brief

Pandey et al. report a mechano-pharmaceutical screening platform for anti-amyloid research, in which a bottom-up strategy recapitulates the hydrophobic core of neurotoxic beta-amyloid (Aβ) oligomers. The single-molecule hydrophobic core is used to screen an NIH library from which 12 inhibitors and 8 stimulators are identified.

INTRODUCTION

Amyloidosis is associated with the deposition of misfolded proteins called amyloids in tissues or organs, which alters the physiological functions of those affected.[1] In Alzheimer disease (AD), the plaques formed by beta-amyloids (Aβ) in brain tissues lead to neurodegenerative symptoms that irreversibly debilitate patients' mental functions over years.[2,3] Drugs available to treat AD include cholinesterase inhibitors[4] and the *N*-methyl-D-aspartate receptor antagonist memantine, which were approved by the US Food and Drug Administration (FDA) decades ago.[5] However, these drugs offer only symptomatic relief while not halting the progression of the disease. To counteract the progression of AD, within the past 20 years, much effort has been focused on disease-modifying drugs, which aim to reduce Aβ generation, prevent Aβ aggregation, or promote Aβ clearance.[6] In 2021, the first Aβ clearance monoclonal antibody, aducanumab,[7] received a conditional approval in the United States for the treatment of AD. However, due to its unclear efficacy and severe side effects, aducanumab was withdrawn from the European market in early 2024 and is only provided with limited availability in the United States at the present time. The second Aβ clearance monoclonal antibody, lecanemab,[8] was approved by the FDA in 2023. Unfortunately, this disease-modifying drug only provides limited symptomatic relief for early AD patients while presenting a range of side effects.[9,10] Given the fact that no effective drug exists to fight AD, it is critical to explore other disease-modifying drugs.

Increasing evidence shows that the pathogenic events of AD originate from the misfolding of the Aβ peptide, followed by sequential nucleation and aggregation of the oligomers, protofibrils, fibrils, and plaques in the brain.[1,2,11] The soluble Aβ oligomers are considered more toxic than the corresponding protofibrils, fibrils, and plaques.[11–15] It is, therefore, desirable to break the train of the Aβ aggregation, especially at the early stage of the oligomers.[11] In fact, many molecules, such as curcumin and epigallocatechin gallate (EGCG), have been found to be effective in disrupting the Aβ aggregation in a screening assay using optical density as the reporting signal.[16,17] After Aβ aggregates into protofibrils or fibrils, they precipitate from the solution, causing decreased light transmittance as the incoming light is scattered off the (proto)fibrils. In an alternative approach, dyes sensitive to the β sheet formation, such as thioflavins, have been used to report the Aβ aggregation.[18,19] It is, however, extremely challenging to cast these two methods onto soluble oligomeric states yet to form β sheets. Other methods have also been reported to surveil the dynamic Aβ oligomerization or to determine whether compounds could prevent Aβ oligomer and fibril formation, such as immunoblotting,[20–22] western blotting,[23–25] and single-molecule fluorescence microscopy.[26–29] However, they either are too laborious for the screening purpose or there is a need to label the Aβ peptide with a large fluorophore, which may significantly vary the oligomerization process relative to unmodified Aβ peptides.[30] Moreover, none of the methods can be used to screen compounds against a single specific target, such as the very first nucleation intermediate leading to Aβ oligomers,[31] which are clinically more relevant due to their demonstrated toxicity.[32,33]

In this work, we demonstrate a new screening strategy to identify small molecules that can interfere with the first step in Aβ nucleation: Aβ dimerization. To simplify the screening design, we chose to use a central motif of the Aβ peptides, FF ($A\beta_{19–20}$), which has

been used as a minimal amyloid model to evaluate known inhibitors that are effective against Aβ aggregation.[34,35] $Aβ_{19–20}$ constitutes the critical region of the hydrophobic core (Lys16-Ala21) in $Aβ_{1–40}$/$Aβ_{1–42}$ peptides and plays an indispensable role in inducing the pathological peptide aggregation.[36–38] As a proof of concept, this dipeptide was chosen to establish a prototypical single-molecule screening platform in which each FF fragment is linked to a 9-mer single-stranded DNA (ssDNA). The two complementary ssDNA strands can hybridize to form a short duplex DNA. Due to the limited Watson-Crick base pair interactions, the formed duplex DNA (double-stranded DNA [dsDNA]) has low stability at room temperature. However, the FF-dimerization increases the thermodynamic stability of the 9-bp duplex DNA, making it feasible to observe the dimerization of the FF dipeptide by mechanical unfolding of individual constructs in an optical tweezers instrument. The mechanical unfolding, in addition, offers a unique angle to probe the interaction between small molecules and the $Aβ_{19–20}$ dimer from a mechanochemical perspective. As hydrophobic contact between $Aβ_{19–20}$ segments is vital to maintain the Aβ oligomer, protofibril, and fibril formation, such mechanical information is highly relevant as neurotoxic Aβ aggregates constantly experience a shear force in blood vessels. Our single-molecule method complements well the thermodynamic, chemical affinity-based conventional screening strategies.

Performing mechanochemical screening against the $Aβ_{19–20}$ dimer formation enabled us to probe different effects of small molecules on the monomer → dimer Aβ association process. We have identified not only new compounds that inhibit the nucleation process but also those that promote the nucleation process. The representative hits were further evaluated in the *in vitro* biophysical and cell assays to confirm the single-molecule screening results. By replacing the $Aβ_{19–20}$ model used in this study with other Aβ-derived sequences (the full hydrophobic core $Aβ_{16–21}$ or the hydrophobic C-terminal fragment $Aβ_{31–42}$), this novel single-molecule screening approach holds promise to identify hit compounds for the treatment of AD in the future. Moreover, given that peptide fragments responsible for aggregation are identified, this new method can also be generalized to investigate the nucleation process of other proteinopathy disorders, which helps researchers discover new molecules that can either interfere with or promote the early amyloid association step critical to the abnormal fibril formation.

RESULTS AND DISCUSSION

Dimerization of diphenylalanine peptides

In conventional assays, FF (i.e., $Aβ_{19–20}$)[34,35] and $Aβ_{1–42}$ peptides have been used to evaluate the Aβ aggregation by signals such as light transmittance or fluorescence dyes specific for β sheet formation (e.g., thioflavin).[39,40] However, these methods do not target oligomers that occur at the early stage of the aggregation (i.e., nucleation). Given the toxicity of the early-stage soluble oligomers,[11,41] these conventional approaches cannot identify the most effective candidates that disrupt early-stage Aβ oligomers. Immunoblotting and western blotting can be used to probe these early-stage oligomers. However, they are limited by their poor sensitivity, slow speed, and laborious procedures.[20–25] To interrogate specific soluble oligomers that dynamically evolve and often exist at low concentrations,

highly sensitive approaches such as single-molecule methods can be applied. Nevertheless, single-molecule techniques are often so sensitive that their signals are overwhelmed by numerous intermediates during the oligomerization of full-length Aβ peptides. For example, single-molecule fluorescence is difficult to deconvolute specific species qualitatively in a mixture of different Aβ oligomers.[26] In addition, the fluorophores used in this technique often have hydrophobic aromatic groups, which may significantly alter the Aβ oligomerization.[30] We hypothesized that using a shorter sequence, such as the hydrophobic core in the full-length Aβ peptide, may be sufficient to establish a prototypical single-molecule screen method. It has been found that diphenylalanine (FF, $A\beta_{19–20}$) plays a critical role in the aggregation of $A\beta_{1–42}$.[38] Experiments have also revealed that $A\beta_{19–20}$ represents the minimalist fragment that can aggregate to form fibrils, showing a high resemblance to amyloid structures.[34,35] The self-assembly of two proximate FF fragments is thus considered a key stepping stone to initiate the Aβ nucleation. Here, we employed this minimal amyloid model to represent the oligomerization and aggregation of full-length Aβ peptides.

However, due to the short length, the FF-dimer formation is expected to be weak and transient, making it difficult to probe by single-molecule approaches. This supposition was confirmed by our initial failure that no FF-dimer formation could be observed at the single-molecule level (data not shown). We reasoned that if we conjugate each FF to the end of each DNA strand in a short duplex DNA, the FF-dimerization and the duplex DNA formation may reinforce each other, leading to a complex dimer that is stable at room temperature. This stable complex dimer can then be easily studied by single-molecule mechanical unfolding in optical tweezers.[42,43] To test this strategy, we first synthesized two molecules (POC1 and POC2) by conjugating FF with DNA strands using microwave-assisted copper-catalyzed alkyne-azide cycloaddition (CuAAC) in a quantitative manner[44–46] (see Figures 1A and S1–S10; Tables S1–S3 for details). To mimic the non-charged $A\beta_{19–20}$ motif, the N-terminal phenylalanine of the FF peptide was acylated, and the C-terminal phenylalanine was amidated. Each peptide-DNA conjugate (POC) contained a DNA domain that can form 9-bp duplex DNA between the two POCs. The DNA strand at the end of each POC is used to ligate to a dsDNA handle (Figure 1B), which can be tethered to an optically trapped bead via one of the affinity linkages (digoxigenin/antibody or biotin/streptavidin) for single-molecule mechanical unfolding experiments (Figure 1C). It is noteworthy that the complex dimer is located opposite to the $poly(thymine(T))_{90}$ spacer, which serves as a linker to hold the two dissociated monomers in proximity. This design allows rapid reassociation of the dimer complex without external force during the incubation, drastically increasing the throughput of the dimerization probing process. The entire DNA-peptide assembly (DPA) was placed within a microfluidic chamber while mechanical folding and unfolding of the FF-dimer were performed to evaluate the association of the $A\beta_{19–20}$ dimer.

After the DPA was tethered between two optically trapped beads, we moved one bead away from another by controlling a steerable mirror that directs one of the trapping lasers. As a result, the tension exerted on the DPA construct was increased, eventually unzipping the DPA dimer to two monomers. However, the dissociation signal of the complex dimer was rare at the loading rate of 5.5 pN/s (in the 10–30 pN range) in a 10-mM Tris buffer containing 100 mM KCl (pH 7.4), indicating that the formation of the complex dimer

under this condition was low. When we increased the loading rate to 15 pN/s in the same Tris buffer with 1 M KCl, unfolding features were clearly observed at 6.7 pN with 98% probability, which was significantly higher than the controls (the dsDNA, dsDNA-5′-FF, and dsDNA-3′-FF) (Figure S11; Table S4). The change-in-contour-length of each rupture event (ΔL = 36 nm) was close to the expected value (37.6 nm, see supplemental experimental procedures for calculations) for the fully extended poly$(T)_{90}$ linker, proving that these rupture features were indeed due to the dissociation of the complex dimer, resulting in a fully extended poly$(T)_{90}$ linker.

To eliminate the possibility that the complex dimer formation was driven by the interaction of the 25-bond linkers between the 9-mer ssDNA and FF, we repeated mechanical unfolding experiments on a control construct assembled from ON1-C5 and ON2-C5 (see Figure S2), which contained the 9-bp DNA duplex and the two interdomain linkers, but without the FF fragments (the dsDNA-25-bond linkers). We observed two unfolding force populations centered at 4.2 and 6.2 pN (Figure S11). While the low force species was likely due to the unzipping of 9-bp dsDNA only (see the 3.9 pN population for the dsDNA), the high force population is close to that of the dissociation for the complex dimers (see the 6.7-pN population for the dsDNA-5′3′FF-dimer). This result suggested that the two 25-bond linkers may also contribute to the POC dimer formation.

To test this hypothesis, we performed molecular dynamics (MD) simulations to obtain molecular insights into the interaction among the DNA, linkers, and FF dipeptides. In the simulations, the structures of all three components were constructed following the same design of the single-molecule mechanical unfolding experiments. The two interdomain linkers were intentionally placed parallel to each other at the beginning of the equilibrium run to observe whether the two linkers could move toward each other in proximity. At the high salt concentration (1 M KCl), we found close proximity between the two linkers, especially for the –CH_2– aliphatic groups, after a 20-ns equilibrium run (Figure 2, panel A1). This is likely due to the ion-induced folding and strong hydrophobic interactions in high salt solutions.[47] We further performed extensive nonequilibrium steered MD (SMD) simulations to evaluate the influence of such strong interactions on the dissociation forces for the DNA-peptide dimer assembly. In the SMD simulations, the two free DNA ends (the ends without connecting to the linker/FF) were connected to driving springs to mimic the dissociation force measurements in experiments. Among 30 independent SMD simulations, we found that the average rupture forces were about 80 pN (Figure 2, panel A2). The magnitudes of the simulated rupture forces were one order of magnitude larger than that of experimental measurements (Figure 3) due to the very high pulling rate in SMD simulation, a well-known timescale issue in the field.[48–50] From the configuration analysis, we found that the two linkers keep binding until the final dissociation (see Figure S12, panel A3 for a typical snapshot). This scenario accounts for about 80% of total SMD runs, indicating that the linker binding makes a large contribution to the interaction of the FF-dimer. As shown in Figure S12, panel A4, we found the intermolecular interactions between the linker and FF peptide were strong during the SMD pulling. Even before the dissociation event, the intermolecular energies of linker/linker and linker/FF were still as large as several kcal/mol (Figure S12, panel A4). All these findings suggested that the linker/linker interaction in a

solution with a high salt concentration (1 M KCl) may complicate the interpretation of the interaction between the ligands and FF-dimers.

The nucleation effect of FF-dimers on the peptide-DNA association

The linker/linker interaction may be reduced if contact time is minimized. To this end, we performed a force jump (FJ) experiment followed by a force-ramping procedure with a high loading rate (15 pN/s) in a Tris buffer with 1 M KCl. During these FJ experiments, the DPA dimer was first mechanically unfolded, followed by a rapid relaxation to 0 pN by an FJ within 10 ms[42] to allow possible refolding of the DPA dimer. After reaching 0 pN, the construct was again force jumped to 1.5 pN, followed by continuous stretching at the 15 pN/s loading rate to evaluate whether the DPA dimer had been formed during the low-force regimes. The entire procedure reduced dwell time for the construct in the low-force regime so that the dimerization of the 25-bond linkers was minimized. Indeed, we found that the two force populations in the “dsDNA-25-bond linkers” construct (Figure S11) reduced to a single species, with its rupture force (5.0 pN; Figure S13) significantly lower than that for the complex dimer dissociation (dsDNA-5′3′FF-dimer, 6.9 pN, $p < 0.001$) by the same FJ procedure in the 1 M KCl buffer.

Since high-salt conditions facilitate hydrophobic interactions that result in the linker/linker association, we reduced the KCl concentration in the buffer. SMD simulation on the mechanical unfolding of the DPA construct in 200 mM KCl solution indeed revealed that the tendency (measured by rupture force) to dimerize two interdomain linkers is much reduced compared to that in 1 M KCl. We did not observe significant linker dimerization after a 20-ns equilibrium run on the DPA construct in 200 mM KCl solution, in complete contrast to that in 1 M KCl solution (see Figure 2B1 for a typical equilibrium configuration in which the two 25-bond linkers largely keep parallel and dissociated to each other). Due to the timescale issue of MD simulation, such a finding does not rule out that the two linkers will never dimerize after a longer time. After performing 30 independent SMD simulations, we found that the average rupture force was about 50 pN (Figure 2B2), significantly lower than that in 1 M KCl solution. Figure S12, panel B3 shows the typical snapshot before the final dissociation of the DPA, which indicates that the rupture force should only be attributed to the interaction between the FF-dimers. Energetic calculations of intermolecular electrostatic and van der Waals interactions between the two linkers or between the linker and the FF peptide along the pulling pathway (Figure S12, panel B4) clearly show that these molecular interactions are negligible compared to those in 1 M KCl solution (Figure S12, panel A4), consistent with the relevant dissociation force histograms.

This result prompted us to further reduce dimerization of the 25-bond linkers in a physiologically more relevant buffer containing 200 mM KCl. To confirm that FF-dimerization occurred in Tris buffer with 200 mM KCl, we first performed non-denaturing gel electrophoresis (Figure S14) and a combined use of molecular modeling and small-angle X-ray scattering (SAXS) (Figures S15–S21; Tables S5–S7) measurements. These experimental results substantiated that 200 mM KCl buffer allowed the orthogonal self-assembly of an FF-dimer on one side and a 9-bp duplex DNA on the other, where each FF was conjugated to one ssDNA via the same interdomain covalent linker.

Next, we carried out regular force-ramping experiments at 15 pN/s loading rate (10–30 pN range). The results still showed that the dsDNA-25-bond linker control had significantly higher dimerization populations (41% formation) than other controls (Figure 3, two center panels, 12%–20% formation). When we performed FJ experiments, the dissociation force of the complex dimer (5.0 pN for the dsDNA-5′3′FF-dimer) was much higher than all the controls (3.1–3.5 pN, $p < 0.001$; Figure 3, right panel), consistent with the FF-dimer formation in the DPA complex. In addition, the differences in the percentage complex dimer formation between the DPA (56% for the dsDNA-5′3’FF) and controls (16%–24%) were much higher than those found in the 1 M KCl buffer (97% vs. ~70% for the DPA vs. controls; Table S4), suggesting that these experimental conditions (FJ coupled with 15 pN/s force loading rate in a buffer with 200 mM KCl) can be exploited to more accurately evaluate the ligand effect on the FF-dimerization. The 56% formation of the complex dimer in the DPA conveniently provides plenty of room to screen and evaluate the compounds that can either inhibit (down to 0%) or promote (up to 100%) the FF-dimerization.

A minimalist mechano-pharmaceutical screening platform for Aβ aggregations

In a typical ligand screening experiment, we first performed FJ experiments on a minimum of three different DPA constructs with at least 100 FJ traces. Based on these data, we calculated the percentage formation of the DPA dimers without inhibitor or promoter molecules in a microfluidic buffer channel (Figure S22). The same DPA construct was then transported to another microfluidic channel that contains a specific compound followed by the FJ experiment to obtain the percentage formation of the complex dimers in the DPA. The two formation percentages were then compared to obtain relative percentages to either promote or inhibit the DPA dimer formation by specific compounds (see the supplemental experimental procedures for calculation).

To validate this evaluation protocol, we chose four molecules, rosmarinic acid (RA), EGCG, tetracycline, and nordihydroguaiaretic acid (NDGA), that have been known to inhibit $A\beta_{1–42}$ aggregations. Similar to the literature report,[34] we found these four compounds inhibit the dimerization of the $A\beta_{19–20}$ (FF) peptides (Figure 4A). To further quantify the potency of these compounds, we evaluated their half-maximal inhibitory concentrations (IC_{50}s) on the FF-dimerization by observing the unfolding events of the complex dimer, as discussed above. To this end, we varied the concentration of each compound while measuring the percentage formation of the complex dimer at a particular inhibitor concentration. We define the percentage formation of the DPA dimer in the buffer channel as the 0% inhibition of the FF-dimerization. In contrast, the 100% inhibition is represented by the percentage formation of the 9-bp duplex DNA conjugated with the 25-bond linkers (i.e., the “dsDNA-25-bond linkers” construct) or the percentage formation that reaches a plateau. Using these two boundary conditions, the relative percentage inhibitory at each concentration of a particular compound was calculated by interpolation (Figure 4A; see the supplemental experimental procedures for details).

After plotting the percentage inhibition vs. compound concentration (Figure 4B), we used the Hill equation (see the supplemental experimental procedures for calculation)[51,52] to retrieve IC_{50}. We found that IC_{50} values of the four compounds were RA (13.1 μM) >

EGCG (26.3 μM) > tetracycline (77.6 μM) > NDGA (107.1 μM). This order matched well with the trend determined by the ensemble turbidity assay,[34] which validated this minimalist screening platform to target Aβ aggregation. Given that our evaluation was based on the dimerization of the $A\beta_{19–20}$ dipeptide, whereas the turbidity assay measured Aβ fibril formation, the similar trend of the four inhibitors suggests the critical importance of the $A\beta_{19–20}$ dimerization during the overall Aβ aggregation processes.

While the $A\beta_{19–20}$ dimerization represents the minimalist platform to mimic Aβ aggregations, evaluating the cohesive mechanical force (i.e., the rupture force measured here) in the $A\beta_{19–20}$ dimer is of unique biological significance. It is known that protein deposits, such as Aβ aggregates, experience shear forces in blood vessels.[53] Thus, we call this minimalist platform mechano-pharmaceutical screening to reflect its capability to identify compounds to reduce the cohesive force in Aβ aggregates, which may lead to dissolutions of the Aβ deposits in blood flow.

Screening an NIH library

Close inspection of the percentage inhibition for the Aβ aggregation vs. concentrations of the four known inhibitors revealed that 100-μM ligands represented significant inhibition of FF dimerization. Therefore, we chose 100 μM to screen a library of druggable compounds provided by the National Institutes of Health (NIH).[54] The results of a total of 121 compounds were summarized in Figure 4C (see Table S8 for FF-dimer formation percentage; Figures S23–S29 for a typical force-extension (FX) curve for each compound). Both inhibitors and promoters of the FF dimerization were found. Compared to RA, 12 compounds showed increased nucleation inhibition. Among these, we found that curcumin has a strong inhibition effect on the FF-dimerization, which is consistent with the literature,[17] further supporting the accuracy of this mechanical screening method. We chose a more potent hit compound, daunorubicin, to obtain IC_{50} by varying the ligand concentration as described above. Indeed, we found a much-reduced IC_{50} (3.5 μM) relative to RA (13.1 μM) (Figure 5A; see Table S8 for the relative formation percentage and calculated relative percentage inhibition at each concentration), confirming the single-molecule screening results. Among the promoters, we also observed a concentration-dependent promotion effect for one of the compounds, ellipticine (Figure 5B; see Table S8 for the relative formation percentage and calculated relative percentage promotion at each concentration). Since ellipticine is a known DNA intercalator,[55] it hints at the possibility that the increased dimer formation could result from facilitated hybridization of the 9-bp dsDNA template due to the ellipticine intercalation. To rule it out, we evaluated the effect of ellipticine on the “dsDNA-25-bond linkers” construct, which showed identical dimer percentage formation with and without the compound. Because ellipticine becomes insoluble in aqueous buffer beyond 200 μM, the IC_{50} can only be estimated for this compound.

To confirm the efficacy of these two compounds on the FF dimerization, we performed a turbidity test (see supplemental experimental procedures section S12 for details). Each inhibitor (6.4 mM) and FF (6.4 mM) was mixed in a MeOH-H_2O (16:84 volume ratio) solution. We found that the inhibitor daunorubicin caused even more reduction in the FF

fiber formation compared to the RA with the same concentration (Figure 5C). However, the promoter ellipticine (with the maximum soluble concentration of 1.2 mM in the methanol-H_2O [16:84 volume ratio]) led to increased FF fiber formation (Figure 5D). These observations are fully consistent with single-molecule screening results.

Next, we subjected the three active small molecules, RA, daunorubicin, and ellipticine, to the thioflavin T (ThT) assay[56] to determine whether their inhibiting or promoting effects against the $A\beta_{19–20}$ aggregation could be cast onto the aggregation of the full-length $A\beta_{1–42}$ peptide (Figure S30), the main disease-causing culprit for AD. To minimize the possible impact on the spontaneous $A\beta_{1–42}$ aggregation, a relatively low concentration of ThT (3.75 μM) was used. This ThT concentration was found to have little influence on the kinetic process of $A\beta_{1–42}$ aggregation when the $A\beta_{1–42}$ concentration was lower than 50 μM.[40] After 24-h incubation, both daunorubicin and RA showed inhibitory effects, with daunorubicin being more potent than RA (Figure 5E), which agreed well with the single-molecule and the clouding assays against the FF dimerization (*vide supra*). Surprisingly, ellipticine gave opposite effects when different concentrations were used (Figures 5F and 5G). At the low-concentration range (≤0.5 μM), ellipticine appeared to be a stimulator (with respect to the positive control of $A\beta_{1–42}$+ThT, normalized fluorescent intensity was 106% for 0.2 μM ellipticine, $p < 0.005$ and 112% for 0.5 μM, ellipticine $p < 0.001$; Figure 5F). After the concentration was increased to >1 μM, inhibition effect was observed for ellipticine against $A\beta_{1–42}$ aggregation. To our knowledge, ellipticine is the first molecule that poses opposite effects to interfere with $A\beta_{1–42}$ aggregation at different concentrations.

Finally, we evaluated the ability of these compounds to protect human microglia cells (C20 cell line) against the $A\beta_{1–42}$ induced toxicity using MTT assays (Figures 5H–5J; see the supplemental experimental procedures for details). The treatment of $A\beta_{1–42}$ (500 nM) significantly decreased the viability of microglia by 43% after 48 h, suggesting that oligomeric $A\beta_{1–42}$ is toxic to neuronal cells. To assess the effect of RA against $A\beta_{1–42}$ induced toxicity, varying concentrations of RA (0.5, 1, and 5 μM) were added to C20 microglia in the presence of $A\beta_{1–42}$ (500 nM). The viability of microglia was significantly increased by up to 17% with the treatment of RA (67% ± 4% viability for 0.5 μM, 66% ± 2% for 1 μM, and 69% ± 2% for 5 μM), compared with the $A\beta_{1–42}$ control group (57% ± 3% viability). The inhibitor daunorubicin showed a toxicity effect by itself and thus cannot be evaluated for its effect on $A\beta_{1–42}$-induced C20 cell toxicity. Protective effects were observed for ellipticine. The viability of $A\beta_{1–42}$-treated microglia was significantly increased by ~14% with the treatment of ellipticine (65% ± 3% viability for 0.05 μM and 64% ± 4% for 0.1 μM), compared with the $A\beta_{1–42}$ control (57% ± 3% viability). This echoed well the promoting effect of ellipticine at the low-concentration range (≤0.5 μM, Figure 5F) in the ThT assay. However, further dose increases of ellipticine did not significantly improve cell viability (61% ± 10% viability for 0.5 μM vs. $A\beta_{1–42}$ control group, $p > 0.05$). It would also be interesting to test the inhibitory effect of ellipticine at the high-concentration range (such as 5 μM; Figure 5G); however, the C20 cell viability became significantly influenced at such high concentrations of ellipticine (Figure S31). Similar results revealed that ellipticine also had protective effects on the neuroblastoma SH-SY5Y cells[57] treated with 10 μM $A\beta_{1–42}$ (Figure S32; supplemental experimental procedures, section S14). To our knowledge, ellipticine has not been reported to be an anti-amyloid

molecule in the literature. We surmise that the protective effect of ellipticine on the C20 and SH-SY5Y cells can be ascribed to its potent stimulation to facilitate fiber formation, which reduced the accumulation of soluble but more toxic oligomers. A similar mechanism has been demonstrated for other small-molecule promoters to protect neurons from toxic Aβ oligomers.[58] The success of identifying ellipticine as a new anti-amyloid compound via the mechano-pharmaceutical screening validated our initial hypothesis of using the core fragment $A\beta_{19–20}$, which is critical to promote $A\beta_{1–42}$ nucleation, to screen a given compound library for anti-amyloid evaluation.

In summary, we have innovated a mechanical screening platform to identify molecules that can interfere with the Aβ aggregation. We have established that FF-dimer serves to nucleate the association of two peptide-oligonucleotide conjugates. Disruption of the FF-dimer therefore may disclose the efficacy of small molecules to either inhibit or promote Aβ aggregations. By screening on an NIH library, we identified various compounds, either inhibitory or stimulatory to Aβ aggregation. Some of these compounds have shown desired effects to target full-length $A\beta_{1–42}$ aggregation by ThT and cell toxicity assays. Among them, ellipticine was identified to act as a stimulator to promote $A\beta_{1–42}$ aggregation at the low-concentration range (≤0.5 μM) but became a potent inhibitor to disrupt $A\beta_{1–42}$ aggregation at the high-concentration range (>1.0 μM).

The present work aimed to establish a prototypical screening assay for anti-amyloid aggregation, a powerful tool to be added to the arsenal of anti-amyloid research. Although our single-molecule screening technique succeeded in identifying a line of anti-amyloid compounds, caveats need to be lodged when extrapolating current results to the full-length Aβ peptides whose behaviors may deviate from the minimalist $A\beta_{19–20}$ dipeptide platform used here. Looking ahead, more specific small-molecule candidates may be identified by replacing the $A\beta_{19–20}$ peptide with longer hydrophobic Aβ-derived fragments like $A\beta_{16–21}$ and $A\beta_{31–42}$.[12,59] The screening against different aggregation-causing hydrophobic fragments may eventually bring about the discovery of lead compound(s) for treating AD. Mean-while, a technically challenging strategy is to substitute the full-length Aβ peptides (e.g., $A\beta_{1–40}$ or $A\beta_{1–42}$) for the FF dipeptide at a single-molecule level to screen effective compounds and elucidate their anti-amyloid aggregation mechanism (the related results will be published in due course). The single-molecule screen method we developed here is not only limited to screen compounds against Aβ aggregation in AD. By substituting the $A\beta_{19–20}$ with other peptide fragments responsible for abnormal protein aggregations, the method can be readily applied to identifying active molecules for the treatment of 35 other types of pathological protein misfolding in difficult-to-cure diseases such as Parkinson, type 2 diabetes, Huntington, and amyotrophic lateral sclerosis.[60]

Due to the inherent properties of the minimalist DPA template, the following cautions must apply to use this mechano-pharmaceutical platform to screen compounds: (1) the peptide fragments should not interact with the DNA double helix or the poly-thymine loop more strongly than that between peptide fragments; (2) the peptide dimer formation templated by the 9-bp DNA duplex must be kinetically faster than the linker dimerization; and (3) intermediate states may emerge to convolute the folding/unfolding pattern when longer peptides are used. Further optimization is required to address these situations.

EXPERIMENTAL PROCEDURES

Details regarding the experimental procedures can be found in the supplemental experimental procedures.

RESOURCE AVAILABILITY

Lead contact

For further information about the single-molecule analysis, please contact Hanbin Mao (hmao@kent.edu).

Materials availability

There are restrictions to the availability of the materials produced in this study for proprietary reasons.

Data and code availability

Data related to the key material preparation and the single-molecule analysis are available in the article and the supplemental information. The raw data are currently not available to third parties for proprietary reasons but will be available from the lead contact upon reasonable request after the proprietary interest is claimed. This paper did not generate any code.

Supplementary Material

Refer to Web version on PubMed Central for supplementary material.

ACKNOWLEDGMENTS

H.M. and C.L. are grateful for financial support from the Lundbeck Foundation, Denmark, grant no. R346–2020-1890. H.M. expresses thanks for the partial support from the NIH (R01CA252827) for this work. C.L. acknowledges the Villum Foundation, Denmark, for funding the Biomolecular Nanoscale Engineering Center (BioNEC), a VILLUM center of excellence, grant no. VKR18333. We acknowledge the European Synchrotron Radiation Facility for the provision of synchrotron radiation facilities, and we would like to thank Erika Foldesne Dudas for assistance and support in using beamline BM29. We thank Seyed Hossein Helalat and Yi Sun for their input into the ThT assay experimental design and result discussion, the lab training, and the access to the GMO labs, as well as the use of the microplate reader at the Department of Health Technology, Technical University of Denmark. This publication was made possible in part by support from the Kent State University Open Access Publishing Fund.

REFERENCES

1. Chiti F, and Dobson CM (2006). Protein misfolding, functional amyloid, and human disease. Annu. Rev. Biochem 75, 333–366. 10.1146/annurev.biochem.75.101304.123901. [PubMed: 16756495]
2. Hardy J, and Selkoe DJ (2002). The amyloid hypothesis of alzheimer's disease: Progress and problems on the road to therapeutics. Science 297, 353–356. 10.1126/science.1072994. [PubMed: 12130773]
3. Blennow K, de Leon MJ, and Zetterberg H (2006). Alzheimer's disease. Lancet 368, 387–403. 10.1016/s0140-6736(06)69113-7. [PubMed: 16876668]
4. Salomone S, Caraci F, Leggio GM, Fedotova J, and Drago F (2012). New pharmacological strategies for treatment of Alzheimer's disease: focus on disease modifying drugs. Br. J. Clin. Pharmacol 73, 504–517. 10.1111/j.1365-2125.2011.04134.x. [PubMed: 22035455]

5. Athar T, Al Balushi K, and Khan SA (2021). Recent advances on drug development and emerging therapeutic agents for Alzheimer's disease. Mol. Biol. Rep 48, 5629–5645. 10.1007/s11033-021-06512-9. [PubMed: 34181171]
6. Reiss AB, Arain HA, Stecker MM, Siegart NM, and Kasselman LJ (2018). Amyloid toxicity in Alzheimer's disease. Rev. Neurosci 29, 613–627. 10.1515/revneuro-2017-0063. [PubMed: 29447116]
7. Dhillon S (2021). Aducanumab: First approval. Drugs 81, 1437–1443. 10.1007/s40265-021-01569-z. [PubMed: 34324167]
8. Cummings J, Apostolova L, Rabinovici GD, Atri A, Aisen P, Greenberg S, Hendrix S, Selkoe D, Weiner M, Petersen RC, and Salloway S (2023). Lecanemab: Appropriate use recommendations. J. Prev. Alzheimers Dis 10, 362–377. 10.14283/jpad.2023.30. [PubMed: 37357276]
9. Lythgoe MP, Jenei K, and Prasad V, (2022). Regulatory decisions diverge over aducanumab for Alzheimer's disease. BMJ 376, e069780. 10.1136/bmj-2021-069780. [PubMed: 35091420]
10. Thambisetty M, and Howard R (2023). Lecanemab trial in AD brings hope but requires greater clarity. Nat. Rev. Neurol 19, 132–133. 10.1038/s41582-022-00768-w. [PubMed: 36609712]
11. Haass C, and Selkoe DJ (2007). Soluble protein oligomers in neurodegeneration: lessons from the Alzheimer's amyloid β-peptide. Nat. Rev. Mol. Cell Biol 8, 101–112. 10.1038/nrm2101. [PubMed: 17245412]
12. Ahmed M, Davis J, Aucoin D, Sato T, Ahuja S, Aimoto S, Elliott JI, Van Nostrand WE, and Smith SO (2010). Structural conversion of neurotoxic amyloid-β_{1-42} oligomers to fibrils. Nat. Struct. Mol. Biol 17, 561–567. 10.1038/nsmb.1799. [PubMed: 20383142]
13. Selkoe DJ (2004). Cell biology of protein misfolding: The examples of Alzheimer's and Parkinson's diseases. Nat. Cell Biol 6, 1054–1061. 10.1038/ncb1104-1054. [PubMed: 15516999]
14. Selkoe DJ, Ihara Y, and Salazar FJ (1982). Alzheimer's disease: Insolubility of partially purified paired helical filaments in sodium dodecyl sulfate and urea. Science 215, 1243–1245. 10.1126/science.6120571. [PubMed: 6120571]
15. Walsh DM, Klyubin I, Fadeeva JV, Rowan MJ, and Selkoe DJ (2002). Amyloid-β oligomers: their production, toxicity and therapeutic inhibition. Biochem. Soc. Trans 30, 552–557. 10.1042/bst0300552. [PubMed: 12196135]
16. Fernandes L, Cardim-Pires TR, Foguel D, and Palhano FL (2021). Green tea polyphenol epigallocatechin-gallate in amyloid aggregation and neurodegenerative diseases. Front. Neurosci 15, 718188. 10.3389/fnins.2021.718188. [PubMed: 34594185]
17. Velander P, Wu L, Henderson F, Zhang S, Bevan DR, and Xu B (2017). Natural product-based amyloid inhibitors. Biochem. Pharmacol 139, 40–55. 10.1016/j.bcp.2017.04.004. [PubMed: 28390938]
18. Biancalana M, and Koide S (2010). Molecular mechanism of thioflavin-T binding to amyloid fibrils. Biochim. Biophys. Acta 1804, 1405–1412. 10.1016/j.bbapap.2010.04.001. [PubMed: 20399286]
19. Dobson CM (1999). Protein misfolding, evolution and disease. Trends Biochem. Sci 24, 329–332. 10.1016/s0968-0004(99)01445-0. [PubMed: 10470028]
20. Zhang Y, and He MI (2017). Deferoxamine enhances alternative activation of microglia and inhibits amyloid beta deposits in APP/PS1 mice. Brain Res 1677, 86–92. 10.1016/j.brainres.2017.09.019. [PubMed: 28963052]
21. Mehta PD, Patrick BA, Barshatzky M, Mehta SP, Frackowiak J, Mazur-Kolecka B, Wegiel J, Wisniewski T, and Miller DL (2018). Generation and partial characterization of rabbit monoclonal antibody to pyro-glutamate amyloid-β_{3-42} (pE_3-Aβ). J. Alzheimers Dis 62, 1635–1649. 10.3233/jad-170898. [PubMed: 29504532]
22. Miller DL, Potempska A, Wegiel J, and Mehta PD (2011). High-affinity rabbit monoclonal antibodies specific for amyloid peptides amyloid-β_{40} and amyloid-β_{42}. J. Alzheimers Dis 23, 293–305. 10.3233/jad-2010-101341. [PubMed: 21116049]
23. Aboukhatwa M, and Luo Y (2011). Antidepressants modulate intracellular amyloid peptide species in N2a neuroblastoma cells. J. Alzheimers Dis 24, 221–234. 10.3233/jad-2011-101113. [PubMed: 21263193]

24. Yao P-L, Zhuo S, Mei H, Chen X-F, Li N, Zhu T-F, Chen S-T, Wang J-M, Hou R-X, and Le Y-Y (2017). Androgen alleviates neurotoxicity of β-amyloid peptide (Aβ) by promoting microglial clearance of Aβ and inhibiting microglial inflammatory response to Aβ. CNS Neurosci. Ther 23, 855–865. 10.1111/cns.12757. [PubMed: 28941188]
25. Taira Y, Inoshima Y, Ishiguro N, Murakami T, and Matsui T (2009). Isolation and characterization of monoclonal antibodies against bovine serum amyloid A1 protein. Amyloid 16, 215–220. 10.3109/13506120903421595. [PubMed: 19922333]
26. Wu J, Cao C, Loch RA, Tiiman A, and Luo J (2020). Single-molecule studies of amyloid proteins: from biophysical properties to diagnostic perspectives. Q. Rev. Biophys 53, e12. 10.1017/S0033583520000086. [PubMed: 33148356]
27. Narayan P, Orte A, Clarke RW, Bolognesi B, Hook S, Ganzinger KA, Meehan S, Wilson MR, Dobson CM, and Klenerman D (2011). The extracellular chaperone clusterin sequesters oligomeric forms of the amyloid-$\beta_{1—40}$ peptide. Nat. Struct. Mol. Biol 19, 79–83. 10.1038/nsmb.2191. [PubMed: 22179788]
28. Dresser L, Hunter P, Yendybayeva F, Hargreaves AL, Howard JAL, Evans GJO, Leake MC, and Quinn SD (2021). Amyloid-β oligomerization monitored by single-molecule stepwise photobleaching. Methods 193, 80–95. 10.1016/j.ymeth.2020.06.007. [PubMed: 32544592]
29. Meng F, Yoo J, and Chung HS (2022). Single-molecule fluorescence imaging and deep learning reveal highly heterogeneous aggregation of amyloid-β 42. Proc. Natl. Acad. Sci. USA 119, e2116736119. 10.1073/pnas.2116736119. [PubMed: 35290118]
30. Wägele J, De Sio S, Voigt B, Balbach J, and Ott M (2019). How fluorescent tags modify oligomer size distributions of the alzheimer peptide. Biophys. J 116, 227–238. 10.1016/j.bpj.2018.12.010. [PubMed: 30638607]
31. Ono K, Condron MM, and Teplow DB (2009). Structure–neurotoxicity relationships of amyloid β-protein oligomers. Proc. Natl. Acad. Sci. USA 106, 14745–14750. 10.1073/pnas.0905127106. [PubMed: 19706468]
32. Cline EN, Bicca MA, Viola KL, and Klein WL (2018). The amyloid-β oligomer hypothesis: Beginning of the third decade. J. Alzheimers Dis 64, S567–S610. 10.3233/jad-179941. [PubMed: 29843241]
33. Lee SJC, Nam E, Lee HJ, Savelieff MG, and Lim MH (2017). Towards an understanding of amyloid-β oligomers: characterization, toxicity mechanisms, and inhibitors. Chem. Soc. Rev 46, 310–323. 10.1039/c6cs00731g. [PubMed: 27878186]
34. Brahmachari S, Arnon ZA, Frydman-Marom A, Gazit E, and Adler-Abramovich L (2017). Diphenylalanine as a reductionist model for the mechanistic characterization of β-amyloid modulators. ACS Nano 11, 5960–5969. 10.1021/acsnano.7b01662. [PubMed: 28575577]
35. Chakraborty P, Bera S, Mickel P, Paul A, Shimon LJW, Arnon ZA, Segal D, Král P, and Gazit E (2022). Inhibitor-mediated structural transition in a minimal amyloid model. Angew. Chem., Int. Ed. Engl 61, e202113845. 10.1002/anie.202113845. [PubMed: 34791758]
36. Reches M, and Gazit E (2005). Self-assembly of peptide nanotubes and amyloid-like structures by charged-termini-capped diphenylalanine peptide analogues. Isr. J. Chem 45, 363–371. 10.1560/5mc0-v3dx-ke0b-yf3j.
37. Kim W, and Hecht MH (2006). Generic hydrophobic residues are sufficient to promote aggregation of the Alzheimer's Aβ42 peptide. Proc. Natl. Acad. Sci. USA 103, 15824–15829. 10.1073/pnas.0605629103. [PubMed: 17038501]
38. Reches M, and Gazit E (2003). Casting metal nanowires within discrete self-assembled peptide nanotubes. Science 300, 625–627. 10.1126/science.1082387. [PubMed: 12714741]
39. Naiki H, Higuchi K, Hosokawa M, and Takeda T (1989). Fluorometric determination of amyloid fibrils in vitro using the fluorescent dye, thioflavine T. Anal. Biochem 177, 244–249. 10.1016/0003-2697(89)90046-8. [PubMed: 2729542]
40. Xue C, Lin TY, Chang D, and Guo Z (2017). Thioflavin T as an amyloid dye: fibril quantification, optimal concentration and effect on aggregation. R. Soc. Open Sci 4, 160696. 10.1098/rsos.160696. [PubMed: 28280572]
41. Benilova I, Karran E, and De Strooper B (2012). The toxic Aβ oligomer and Alzheimer's disease: an emperor in need of clothes. Nat. Neurosci 15, 349–357. 10.1038/nn.3028. [PubMed: 22286176]

42. Koirala D, Dhakal S, Ashbridge B, Sannohe Y, Rodriguez R, Sugiyama H, Balasubramanian S, and Mao H (2011). A single-molecule platform for investigation of interactions between G-quadruplexes and small-molecule ligands. Nat. Chem 3, 782–787. 10.1038/nchem.1126. [PubMed: 21941250]
43. Pandey S, Mandal S, Danielsen MB, Brown A, Hu C, Christensen NJ, Kulakova AV, Song S, Brown T, Jensen KJ, et al. (2022). Chirality transmission in macromolecular domains. Nat. Commun 13, 76. 10.1038/s41467-021-27708-4. [PubMed: 35013247]
44. Ejlersen M, Christensen NJ, Sørensen KK, Jensen KJ, Wengel J, and Lou C (2018). Synergy of two highly specific biomolecular recognition events: Aligning an AT-hook peptide in DNA minor grooves via covalent conjugation to 2'-amino-LNA. Bioconjugate Chem 29, 1025–1029. 10.1021/acs.bioconjchem.8b00101.
45. Danielsen MB, Christensen NJ, Jørgensen PT, Jensen KJ, Wengel J, and Lou C (2021). Polyamine-functionalized 2′-amino-lna in oligonucleotides: Facile synthesis of new monomers and high-affinity binding towards ssDNA and dsDNA. Chem. Eur J 27, 1416–1422. 10.1002/chem.202004495. [PubMed: 33073896]
46. Fantoni NZ, El-Sagheer AH, and Brown T (2021). A hitchhiker's guide to click-chemistry with nucleic acids. Chem. Rev 121, 7122–7154. 10.1021/acs.chemrev.0c00928. [PubMed: 33443411]
47. Yoda T, Sugita Y, and Okamoto Y (2014). Salt effects on hydrophobic-core formation in folding of a helical miniprotein studied by molecular dynamics simulations. Proteins 82, 933–943. 10.1002/prot.24467. [PubMed: 24214490]
48. Li P-C, and Makarov DE (2003). Theoretical studies of the mechanical unfolding of the muscle protein titin: Bridging the time-scale gap between simulation and experiment. J. Chem. Phys 119, 9260–9268. 10.1063/1.1615233.
49. Park S, Khalili-Araghi F, Tajkhorshid E, and Schulten K (2003). Free energy calculation from steered molecular dynamics simulations using Jarzynski's equality. J. Chem. Phys 119, 3559–3566. 10.1063/1.1590311.
50. Park S, and Schulten K (2004). Calculating potentials of mean force from steered molecular dynamics simulations. J. Chem. Phys 120, 5946–5961. 10.1063/1.1651473. [PubMed: 15267476]
51. DeLean A, Munson PJ, and Rodbard D (1978). Simultaneous analysis of families of sigmoidal curves: application to bioassay, radioligand assay, and physiological dose-response curves. Am. J. Physiol 235, E97–E102. 10.1152/ajpendo.1978.235.2.E97. [PubMed: 686171]
52. Gesztelyi R, Zsuga J, Kemeny-Beke A, Varga B, Juhasz B, and Tosaki A (2012). The Hill equation and the origin of quantitative pharmacology. Arch. Hist. Exact Sci 66, 427–438. 10.1007/s00407-012-0098-5.
53. Scheres SHW, Ryskeldi-Falcon B, and Goedert M (2023). Molecular pathology of neurodegenerative diseases by cryo-EM of amyloids. Nature 621, 701–710. 10.1038/s41586-023-06437-2. [PubMed: 37758888]
54. Pal R, and Seleem MN (2020). Screening of natural products and approved oncology drug libraries for activity against *clostridioides difficile*. Sci. Rep 10, 5966. 10.1038/s41598-020-63029-0. [PubMed: 32249833]
55. Řeha D, Kabelác M, Ryjácek F, Šponer J, Šponer JE, Elstner M, Suhai S, and Hobza P (2002). Intercalators. 1. Nature of stacking interactions between intercalators (ethidium, daunomycin, ellipticine, and 4',6-diaminide-2-phenylindole) and DNA base pairs. Ab initio quantum chemical, density functional theory, and empirical potential study. J. Am. Chem. Soc 124, 3366–3376. 10.1021/ja011490d. [PubMed: 11916422]
56. Kwon Y, Shin J, Nam K, An JS, Yang S-H, Hong S-H, Bae M, Moon K, Cho Y, Woo J, et al. (2020). Rhizolutin, a novel 7/10/6-tricyclic dilactone, dissociates misfolded protein aggregates and reduces apoptosis/inflammation associated with Alzheimer's disease. Angew. Chem., Int. Ed. Engl 59, 22994–22998. 10.1002/anie.202009294. [PubMed: 32844539]
57. Song Z, He C, Yu W, Yang M, Li Z, Li P, Zhu X, Xiao C, and Cheng S (2022). Baicalin attenuated $A\beta_{1-42}$-Induced apoptosis in SH-SY5Y cells by inhibiting the Ras-ERK signaling pathway. BioMed Res. Int 2022, 9491755. 10.1155/2022/9491755. [PubMed: 35528169]
58. Bieschke J, Herbst M, Wiglenda T, Friedrich RP, Boeddrich A, Schiele F, Kleckers D, Lopez del Amo JM, Grüning BA, Wang Q, et al. (2011). Small-molecule conversion of toxic oligomers

to nontoxic β-sheet–rich amyloid fibrils. Nat. Chem. Biol 8, 93–101. 10.1038/nchembio.719. [PubMed: 22101602]

59. Colletier J-P, Laganowsky A, Landau M, Zhao M, Soriaga AB, Goldschmidt L, Flot D, Cascio D, Sawaya MR, and Eisenberg D (2011). Molecular basis for amyloid-β polymorphism. Proc. Natl. Acad. Sci. USA 108, 16938–16943. 10.1073/pnas.1112600108. [PubMed: 21949245]
60. Ross CA, and Poirier MA (2004). Protein aggregation and neurodegenerative disease. Nat. Med 10, S10–S17. 10.1038/nm1066. [PubMed: 15272267]

Highlights

- A single-molecule mechanical screening platform for anti-amyloid research
- identified 12 inhibitors and 8 stimulators from an NIH compound library
- Anti-amyloid activities of hit compounds confirmed in cell assays
- Screening method is readily extensible to other proteinopathies

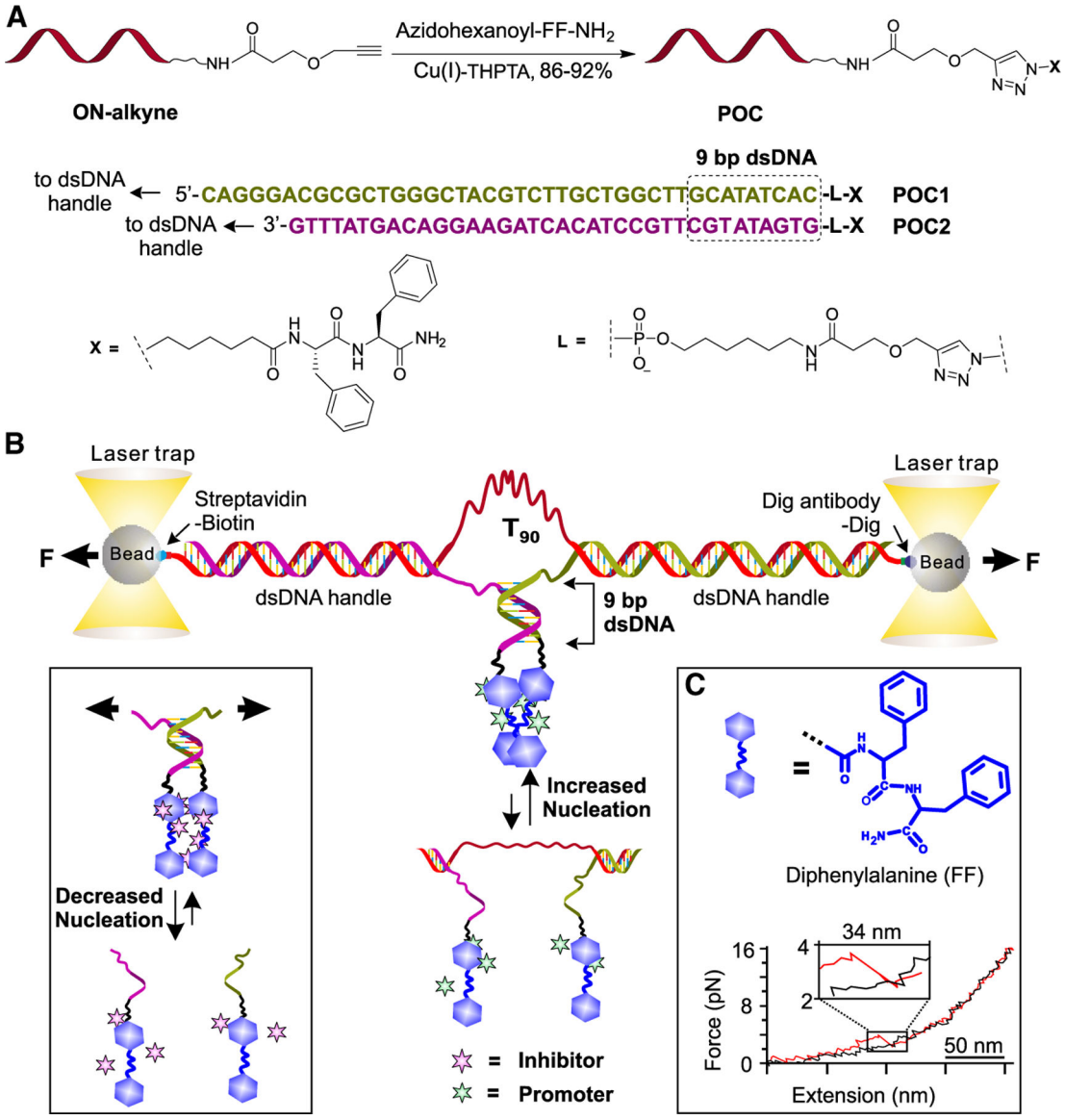

Figure 1. Design of mechano-pharmaceutical screening platform

(A) A schematic diagram for the synthesis of POCs via the microwave-assisted CuAAC reactions.

(B) Schematic drawing of the single-molecule platform to investigate the $A\beta_{19–20}$ (FF) dimerization under promoter molecules. The left inset shows the effect of inhibitor molecules on the $A\beta_{19–20}$ dimerization.

(C) Top, representation of FF and its structure. Bottom, typical force-extension (FX) curves (loading rate 15 pN/s in 10–30 pN range) with dissociation events for the DNA-peptide dimer assembly in 10 mM Tris buffer (pH 7.4) supplemented with 200 mM KCl (bottom).

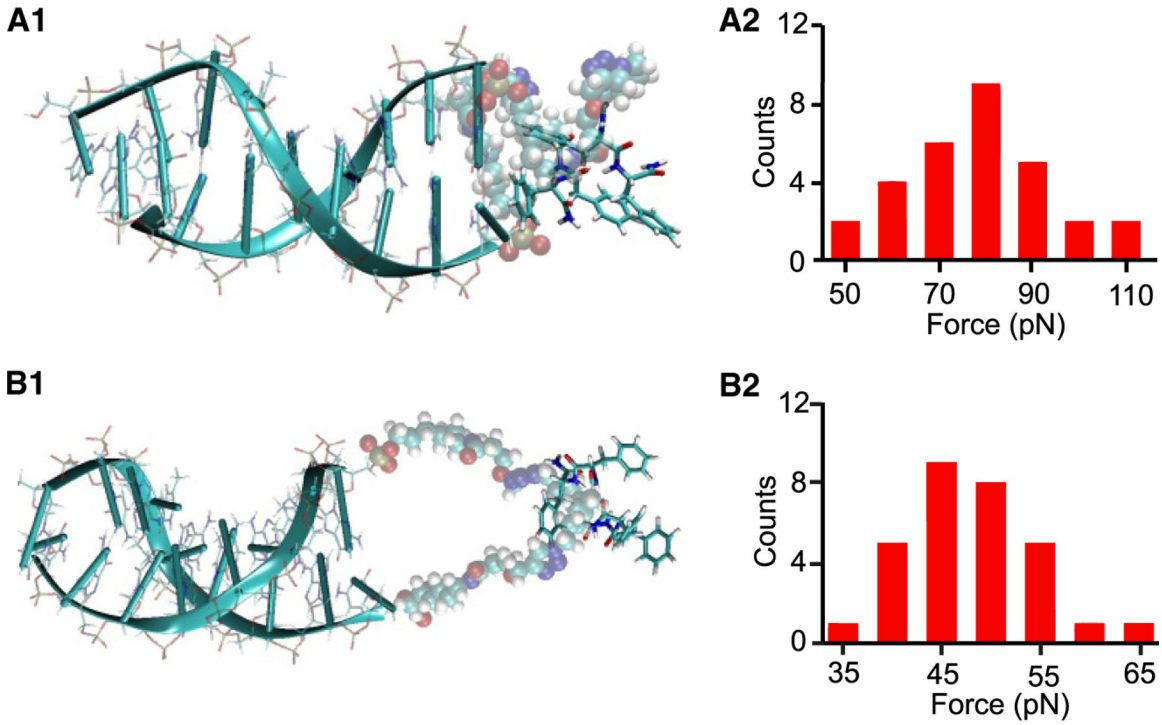

Figure 2. Molecular dynamics (MD) simulations of DNA-peptide dimer assembly

(A1) Typical snapshot showing the equilibrium configuration of the DNA-peptide dimer assembly with linkers in 1 M KCl solution. To distinguish each part of the assembly, we use opaque ribbons and transparent sticks to represent the short duplex DNA and transparent spheres to show the linkers. FF peptides are shown in opaque sticks.

(A2) Dissociation force histograms for the DNA-peptide dimer assembly in 1 M KCl solution.

(B1 and B2) Corresponding results in 200 mM KCl solution. In all molecular configurations, water molecules and ions are not shown for clarity. Color key: red, O; white, H; light blue, C; dark blue, N.

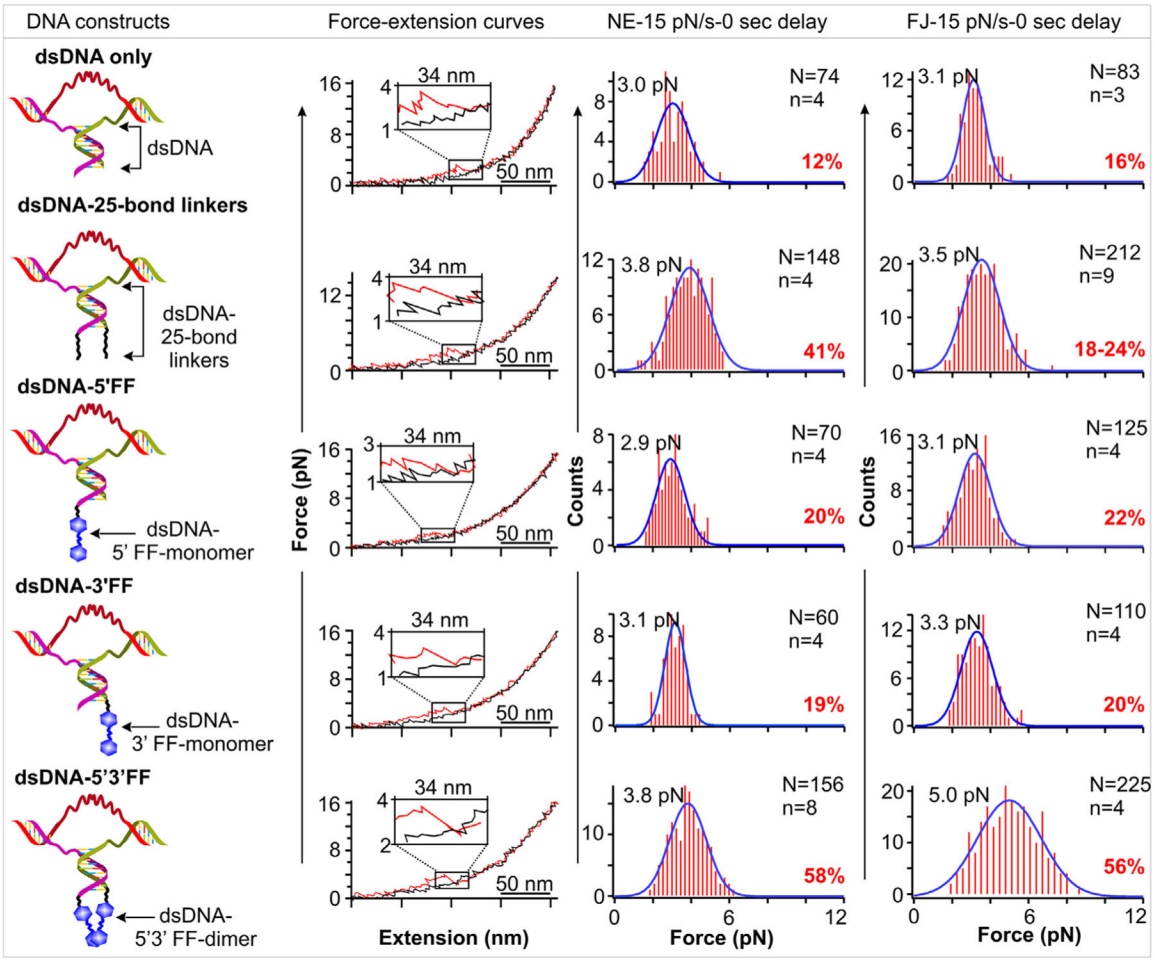

Figure 3. Mechanical stability and percentage formation of various duplex DNA constructs with and without $A\beta_{19-20}$ dimerization

(Left column) Schematic drawing for each construct. (Center column) Typical FX curves in 10 mM Tris buffer supplemented with 200 mM KCl (pH 7.4). (Right two columns) Dissociation force histograms for force ramping normal experiments (NE) and force jump (FJ) experiments, respectively. In both experiments, the loading rate was kept at 15 pN/s, while incubation time was set as 0 s to reduce the dimerization of the 25-bond linkers between each 9-mer DNA and the FF peptide. *N* and *n* represent the number of curves and the number of DPA constructs, respectively. The percentage formation of respective dimer in each construct is depicted in red. Exact formation percentages vary with different optical tweezers instruments. For example, they show a range between 18% and 24% for the "dsDNA-25-bond linkers" construct in the FJ mode.

A

Inhibitors / Conc (mM)	Formation% (%Inhibition)							
	0	1	3	10	30	100	300	1000
RA	52 (0)	48 (9)	53 (19)	41 (47)	—	31 (89)	—	29 (100)
EGCG	52 (0)	50 (11)	54 (24)	42 (46)	—	33 (94)	31 (100)	—
NDGA	50 (0)	—	—	48 (12)	55 (25)	42 (58)	36 (85)	32 (100)
Tetracycline	52 (0)	—	—	48 (10)	45 (32)	40 (62)	34 (95)	30 (100)

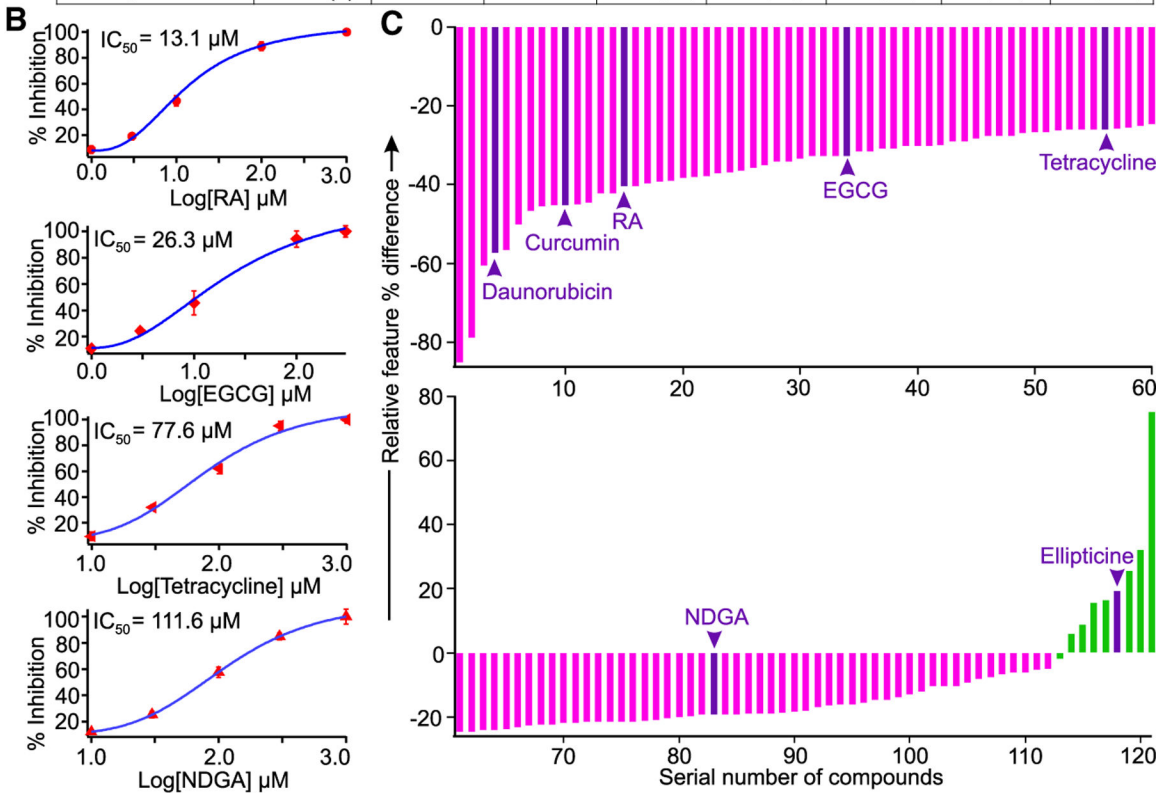

Figure 4. Mechano-pharmaceuticalscreening of small molecules against FF-dimer association

(A) Formation percentage (percentage inhibition) of dsDNA-FF-dimers in presence of four inhibitors at different concentrations. The formation percentage and percentage inhibition were calculated by Equations S4 and S5, respectively (see supplemental information for details).

(B) Inhibitory curves of four known inhibitors against FF-dimerization. IC_{50} was calculated by the Hill equation (see supplemental information for details). Error bars depict SDs from at least three independent measurements of different molecules.

(C) Screening of an NIH library to identify inhibitory (pink) and stimulatory (green) compounds for the FF-dimerization. Known inhibitors are shown in purple.

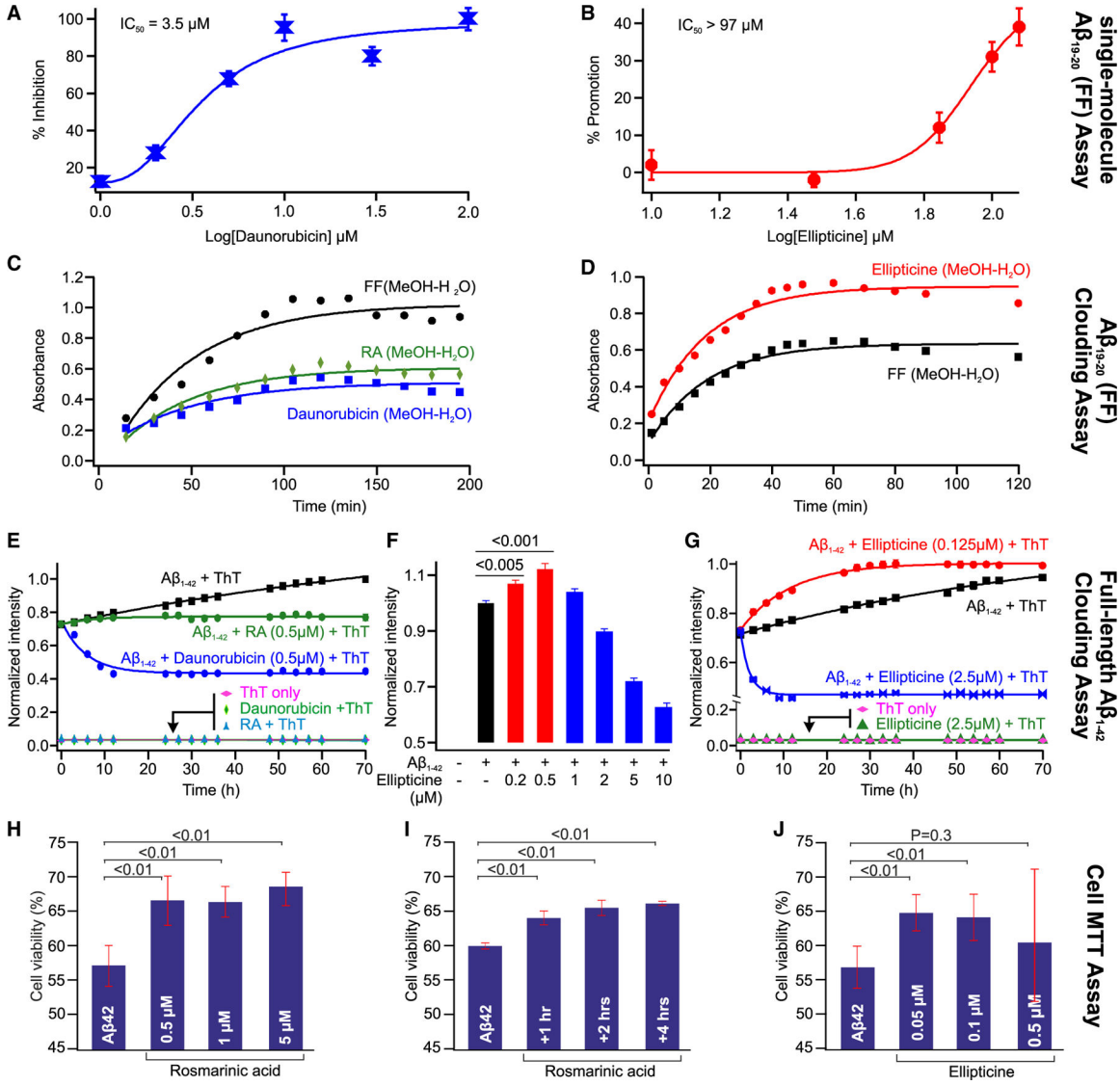

Figure 5. Characterization of the compounds screened by the mechano-pharmaceutical platform

(A) IC_{50} inhibition measurement of daunorubicin.

(B) Promotion effect of ellipticine to increase the FF-dimer formation. Error bars depict SDs from at least three independent measurements of different molecules. IC_{50} was calculated by the Hill equation in (A) and (B) (see supplemental information for details).

(C and D) Turbidity assays of FF (6.4 mM) with RA (6.4 mM) and daunorubicin (6.4 mM) (C) and those of FF (1.2 mM) and ellipticine (1.2 mM) (D).

(E) Real-time clouding assays of $A\beta_{1–42}$ (6.25 μM) aggregation revealed by fluorogenic ThT (3.75 μM) with or without RA (0.5 μM) or daunorubicin (0.5 μM).

(F) A clouding assay of preincubating $A\beta_{1–42}$ (25 μM) with varied ellipticine concentrations (0–10 μM) for 24 h, which was then revealed by fluorogenic ThT (3.75 μM).

(G) Real-time clouding assays of $A\beta_{1–42}$ (6.25 μM) aggregation revealed by fluorogenic ThT (3.75 μM) with ellipticine (0.125 μM and 2.5 μM).

For (E)–(G), Aβ aggregation was reported to preserve the same kinetic process when ≤50 μM $A\beta_{1-42}$ and ≤20 μM ThT were used.[40]

(H–J) Viability of human microglial cells (C20) under different doses (H) and time of incubation at 1 μM (I) of RA and ellipticine compounds (J).

At least three independent experiments were repeated for (H)–(J). In each repeat, 10 technical replicates were performed. Error bars represent SDs. In (C)–(E) and (G), solid curves depict exponential fittings to guide eyes.